ISSN 1674-1056
http://cpb.iphy.ac.cn
http://iopscience.iop.org/cpb
中国物理 B
Chinese Physics
中国物理
Chinese Physics B

Signatures of strong interlayer coupling in γ-InSe revealed by local differential conductivity

Xiaoshuai Fu(富晓帅), Li Liu(刘丽), Li Zhang(张力), Qilong Wu(吴奇龙), Yu Xia(夏雨), Lijie Zhang(张利杰), Yuan Tian(田园), Long-Jing Yin(殷隆晶), and Zhihui Qin(秦志辉)

Citation: Chin. Phys. B, 2021, 30 (**8**): 087306. DOI: 10.1088/1674-1056/abff32
Journal homepage: http://cpb.iphy.ac.cn; http://iopscience.iop.org/cpb

What follows is a list of articles you may be interested in

Giant Rashba-like spin-orbit splitting with distinct spin texture in two-dimensional heterostructures

Jianbao Zhu(朱健保), Wei Qin(秦维), and Wenguang Zhu(朱文光)
Chin. Phys. B, 2021, 30 (**8**): 087307. DOI: 10.1088/1674-1056/ac0784

Progress on band structure engineering of twisted bilayer and two-dimensional moirè heterostructures

Wei Yao(姚维), Martin Aeschlimann, and Shuyun Zhou(周树云)
Chin. Phys. B, 2020, 29 (**12**): 127304. DOI: 10.1088/1674-1056/abc7b6

Emerging properties of two-dimensional twisted bilayer materials

Yang Cheng(程阳), Chen Huang(黄琛), Hao Hong(洪浩), Zixun Zhao(赵子荀), Kaihui Liu(刘开辉)
Chin. Phys. B, 2019, 28 (**10**): 107304. DOI: 10.1088/1674-1056/ab3e46

Electronic properties of silicene in BN/silicene van der Waals heterostructures

Ze-Bin Wu(吴泽宾), Yu-Yang Zhang(张余洋), Geng Li(李更), Shixuan Du(杜世萱), Hong-Jun Gao(高鸿钧)
Chin. Phys. B, 2018, 27 (**7**): 077302. DOI: 10.1088/1674-1056/27/7/077302

Topological edge states and electronic structures of a 2D topological insulator: Single-bilayer Bi (111)

Gao Chun-Lei, Qian Dong, Liu Can-Hua, Jia Jin-Feng, Liu Feng
Chin. Phys. B, 2013, 22 (**6**): 067304. DOI: 10.1088/1674-1056/22/6/067304

RAPID COMMUNICATION

Signatures of strong interlayer coupling in γ-InSe revealed by local differential conductivity*

Xiaoshuai Fu(富晓帅), Li Liu(刘丽), Li Zhang(张力)†, Qilong Wu(吴奇龙), Yu Xia(夏雨), Lijie Zhang(张利杰), Yuan Tian(田园), Long-Jing Yin(殷隆晶), and Zhihui Qin(秦志辉)‡

Key Laboratory for Micro/Nano Optoelectronic Devices of Ministry of Education & Hunan Provincial Key Laboratory of Low-Dimensional Structural Physics and Devices, School of Physics and Electronics, Hunan University, Changsha 410082, *China*

(Received 21 April 2021; revised manuscript received 28 April 2021; accepted manuscript online 8 May 2021)

Interlayer coupling in layered semiconductors can significantly affect their optoelectronic properties. However, understanding the mechanisms behind the interlayer coupling at the atomic level is not straightforward. Here, we study modulations of the electronic structure induced by the interlayer coupling in the γ-phase of indium selenide (γ-InSe) using scanning probe techniques. We observe a strong dependence of the energy gap on the sample thickness and a small effective mass along the stacking direction, which are attributed to strong interlayer coupling. In addition, the moiré patterns observed in γ-InSe display a small band-gap variation and nearly constant local differential conductivity along the patterns. This suggests that modulation of the electronic structure induced by the moiré potential is smeared out, indicating the presence of a significant interlayer coupling. Our theoretical calculations confirm that the interlayer coupling in γ-InSe is not only of the van der Waals origin, but also exhibits some degree of hybridization between the layers. Strong interlayer coupling might play an important role in the performance of γ-InSe-based devices.

Keywords: indium selenide (InSe), interlayer coupling, scanning tunneling microscopy/spectroscopy (STM/STS), density functional theory

PACS: 73.20.At, 68.37.Ef, 71.15.Mb **DOI:** 10.1088/1674-1056/abff32

1. Introduction

Interlayer coupling plays an important role in determining the properties of layered semiconductors.[1–8] As one of the representative III–VI layered semiconductors, indium selenide (InSe) demonstrates attractive electronic transport properties with high carrier mobility, quantum Hall effect, and broadband optical response ranging from ultraviolet to near-infrared due to the high tunability of the band gap.[9–14] As the number of InSe layers increases, the band gap reduces, which is accompanied by a transition from an indirect to direct band gap.[15–17] Large variations of the InSe band structure with thickness were considered to be originating from the strong interlayer coupling due to the Se p_z orbitals.[18–20] Therefore, both theoretical and experimental studies pay great attention to the interlayer coupling and related phenomena in InSe.[18,21,22] Sun *et al*. demonstrated that InSe is a strongly coupled layered material by employing *ab initio* density functional (DFT) calculations.[18] The peak position and linewidth of the excitonic emission from mechanically exfoliated InSe flakes with various thicknesses were reported earlier to elaborate the interlayer coupling.[21] Afterwards, Mudd *et al*. investigated highly tunable optical response and spectral variation with external magneto-optical fields applying to the InSe samples.[22] It was also reported that the band structure of InSe could be tuned by uniaxial tensile strain or doping, and the induced modification of interlayer coupling might be the origin.[19,23] Such interlayer coupling was likewise involved in a study of InSe-based hot-carrier optoelectronics.[24] However, particular efforts should place emphasis on the influence of interlayer coupling on localized electronic band gaps, which is critical for related optoelectronics.[25,26] Scanning probe techniques give access to the differential conductivities, which are directly associated with the local electronic states and band gaps of samples,[27,28] and therefore may be useful to understand the physics of interlayer coupling in InSe at the atomic level.

In this paper, we study the γ-phase of InSe (γ-InSe) by using scanning tunneling microscope/spectroscopy (STM/STS). γ-InSe samples with different thicknesses ranging from a few layers to hundreds of nanometers, as well as the bulk crystal are used in the measurements. We observe a sharp drop of the band gap when the sample thickness increases, which suggests strong interlayer coupling in γ-InSe. This is further corroborated by a small effective mass and large exciton radius along the out-of-plane direction extracted from the differential conductivity measurements. We also observe the moiré patterns indicating the presence of a superlattice with a $\sim 7.3^\circ$

*Project supported by the National Natural Science Foundation of China (Grant Nos. 51772087, 11804089, 11574350, 11904094, and 51972106), the Natural Science Foundation of Hunan Province, China (Grant Nos. 2018JJ3025, 2019JJ50034, and 2019JJ50073), the Strategic Priority Research Program of Chinese Academy of Sciences (Grant No. XDB30000000), and the Fundamental Research Funds for the Central Universities of China.

†Corresponding author. E-mail: li_zhang@hnu.edu.cn

‡Corresponding author. E-mail: zhqin@hnu.edu.cn

© 2021 Chinese Physical Society and IOP Publishing Ltd

twist angle between the surface layer and the underlying layers, where the slightly larger band gap than that of bulk γ-InSe is the signature of a considerable interlayer coupling. Our results demonstrate that the moiré-pattern-related band-gap features do not exhibit stack-dependent variations, which reveals the strong interlayer coupling induced smearing of the moiré potential modulation along the layer. Our work highlights that the strong interlayer coupling can efficiently affect the electronic properties of γ-InSe, which provides further insights for applications.

2. Materials and methods

2.1. Sample preparation and characterization

The γ-InSe sample with different thickness was prepared by gold-assisted mechanical exfoliation method.[29] First, an adhesion metal layer (Ti, 5 nm) is evaporated on Si substrate (with 300 nm SiO_2 film), then Au film (15 nm) is deposited on the substrate. The fresh surface of the γ-InSe crystal is cleaved by a tape and put onto the metal-deposited substrate. The tape removes from the substrate after pressing vertically for about 1 min to obtain large-area γ-InSe sheets. Bulk InSe (2D semiconductors USA) was repeatedly surface cleaved in the ambient atmosphere and quickly loaded to ultrahigh vacuum followed by the 20 min degas at 450 K.

All experiments were performed with a commercial STM (CreaTec Fischer & Co. GmbH) with ultrahigh vacuum ($\sim 2\times10^{-10}$ Torr) and low temperature ($\sim$ 77 K). STM images were processed using WSxM.[30] All $\mathrm{d}I/\mathrm{d}V$ spectra were acquired by utilizing the internal lock-in amplifier with the modulation voltage of 50 mV at the frequency of 739 Hz. STM images were taken in the constant-current mode with the sample biased. Electrochemically etched PtIr/W tips calibrated on Au(111) surface beforehand were used in STM/STS experiments. Raman measurements were performed in a Renishaw inVia Raman microscope equipped with a 532 nm laser. Atomic force microscope (Park Systems Corp.) experiments were performed under ambient conditions with the tapping mode.

3. Theoretical calculations

The density functional theory calculations were carried out using the projected augmented wave formalism[31] as implemented in the Vienna *ab initio* simulation package (VASP).[32,33] The exchange–correlation effects were taken into account by using the local density approximation (LDA). A 250 eV energy cutoff for the plane-waves and a convergence threshold of 10^{-6} eV have been used. The Brillouin zone was sampled by (16×16) and (2×2) k-point meshes for non-twisted and twisted bilayers, respectively. In order to avoid interactions between the supercell structures in the nonperiodic direction, a 30 Å thick vacuum slab was added in the direction normal to the InSe plane. The atomic positions in the twisted supercell were relaxed until the residual forces were less than 10^{-2} eV/Å. The unit cell of InSe was optimized at the LDA level, resulting in the lattice constant $a = 3.95$ Å. The supercell of twisted bilayer InSe was constructed using the lattice vectors $\boldsymbol{t}_1 = n\boldsymbol{a}_1 + m\boldsymbol{a}_2$ and $\boldsymbol{t}_2 = (n+m)\boldsymbol{a}_1 - m\boldsymbol{a}_2$ rotated by angles $\theta/2$ and $-\theta/2$, respectively. Here, $\boldsymbol{a}_1$ and $\boldsymbol{a}_2$ are the lattice vectors of the InSe unit cell, and θ is the twist angle determined by a common periodicity of the two layers, satisfying[34]

$$\cos(\theta) = \frac{\left(2n^2+2nm-m^2\right)}{2\left(n^2+nm+m^2\right)}. \tag{1}$$

In this work, we consider $n = 5$ and $m = 4$, giving rise to the twist angle $\theta = 7.34^\circ$. The resulting periodicity is $a_{\mathrm{twist}} = a\sqrt{m^2+nm+n^2} \simeq 30.9$ Å, whereas the supercell has 488 atoms. The Wannier functions were constructed using the wannier90 package.[35]

4. Results and discussion

The ball-and-stick model of γ-InSe with top and side views is shown in Fig. 1(a). It has a hexagonal structure from the top view with the lattice parameter $a = 0.4$ nm and the C_{3v} point-group symmetry.[36,37] From the side view, quadruple-layer (QL) γ-InSe with a thickness of about 0.8 nm consists of four atomic monolayers linked via covalent bonds in the sequence of Se–In–In–Se, and 3QL forms the unit cell with lattice parameter $c = 2.5$ nm along the perpendicular direction together with an in-plane shift. The thickness of 1QL γInSe is verified by large-scale STM images as the line profile across the terrace edge gives a height of ~ 0.8 nm [Fig. 1(b)]. The surface structure of γ-InSe is well identified by the atomically resolved STM image of the bulk sample [Fig. 1(c)]. The characteristic honeycomb structure has a lattice parameter of ~ 0.4 nm, which is consistent with the γ-InSe model. The corresponding Raman spectroscopy [Fig. 1(d)] verified the γ-phase. Four dominant peaks centered at ~ 114 cm^{-1} (A_1'), 176 cm^{-1} (E′-TO and E″), 199 cm^{-1} (A_2''-LO), and 226 cm^{-1} (A_1') are characteristic peaks for the γ-phase, which are in good agreement with the literature.[38]

A series of γ-InSe sheets were mechanically exfoliated from the γ-phase bulk crystal onto the Au/Ti/SiO_2/Si substrate to examine the band gap dependence on the sample thickness. Utilizing the *in-situ* long distance microscope to identify the tip positions, we measured the differential conductance ($\mathrm{d}I/\mathrm{d}V$) spectra on specific γ-InSe sheets, whose thickness was accurately determined beforehand by means of the atomic force microscopy (see supporting information for details). All band gap values extracted from $\mathrm{d}I/\mathrm{d}V$ curves including those for bulk γ-InSe are plotted in Fig. 2(a) with black squares,

whereas three typical dI/dV curves acquired for regions 1, 5, and 11 (defined in supporting information) are shown in Fig. 2(b) as references. A relatively sharp drop of the band gap from ~ 2.5 to ~ 1.4 eV is clearly observed when the thickness of γ-InSe sheets increases from a single layer to ~ 20 nm. The band gap remains nearly constant (~ 1.2 eV) for thicknesses above ~ 20 nm, which corresponds to that of bulk γ-InSe. The calculated band gaps for 2QL, 3QL, and bulk γ-InSe are also labeled by stars in Fig. 2(a), exhibiting the same decreasing trend as in the experiment. In contrast to transition metal dichalcogenides,[39] strong dependence of a band gap on the number of layers is a manifestation of strong interlayer coupling in γ-InSe,[18] where quantum confinement alone is not sufficient to explain the sharp drop of the band gap. In order to gain further insight into the band gap variation with thickness, we adopt the effective mass model[21]

$$E_g = E_0 + \frac{\pi^2\hbar^2}{2m^*d^2}, \tag{2}$$

where $E_0 = 1.2$ eV is the band gap of bulk γ-InSe measured in our experiment, m^* is the out-of-plane effective mass of bulk γ-InSe along the k_z direction, and $\hbar$ is the reduced Planck's constant. The fitting gives the effective mass of $\sim 0.06m_e$ (m_e is the free electron mass), which is quite small among the layered semiconductors and consistent with previous results.[21,40] A small out-of-plane effective mass implies a highly dispersive behavior along the k_z direction at the K point, which is in line with previous theoretical calculations.[41] We further find that the Wannier–Mott exciton radius (r) in γ-InSe reaches ~ 11 nm by[42]

$$\frac{m^*}{m_e} = \frac{\varepsilon a_B}{r_0}, \tag{3}$$

where $a_B = 53$ pm is the Bohr radius and $\varepsilon = 11.6$ is the dielectric constant of γ-InSe.[43] The exciton radius is the characteristic length scale of quantum effects presenting in the system. One can see that r is smaller than the γ-InSe thickness threshold, at which the band gap displays a clear modification [see Fig. 2(a)]. In this situation, quantum confinement is not significant when the thickness is decreased down to ~ 20 nm, and strong interlayer coupling should be the major factor resulting in the fast band gap enhancement with decreasing thickness. The large exciton radius also indicates a bulk-like character of charge carriers, which is considered to be a sign of strong interlayer coupling in γ-InSe.

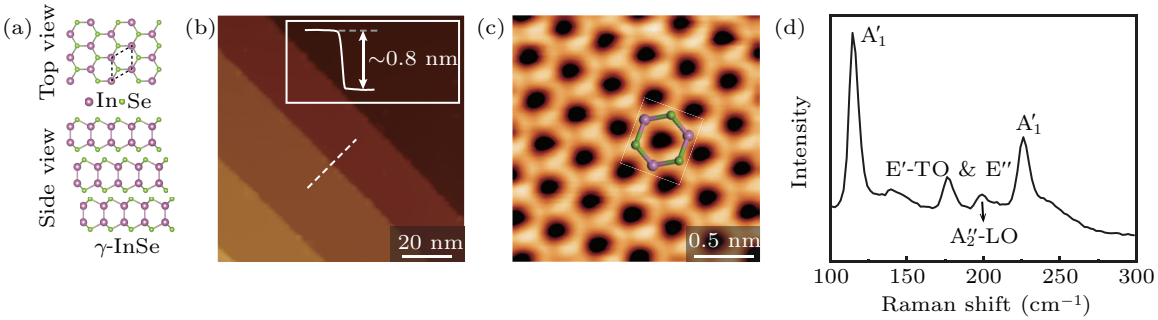


Fig. 1. (a) The ball-and-stick model of γ-InSe with top view (upper panel) and side view (lower panel). The dashed rhombus in (a) represents the in-plane primitive cell. (b) Large-scale STM image (2 V, 2 pA) of the typical γ-InSe surface. The inset shows the height profile along the dashed line providing a height of ~ 0.8 nm for 1QL γ-InSe. (c) Atomic-resolution STM image (1.5 V, 10 pA) of the exfoliated γ-InSe crystal. (d) Raman spectra of γ-InSe.

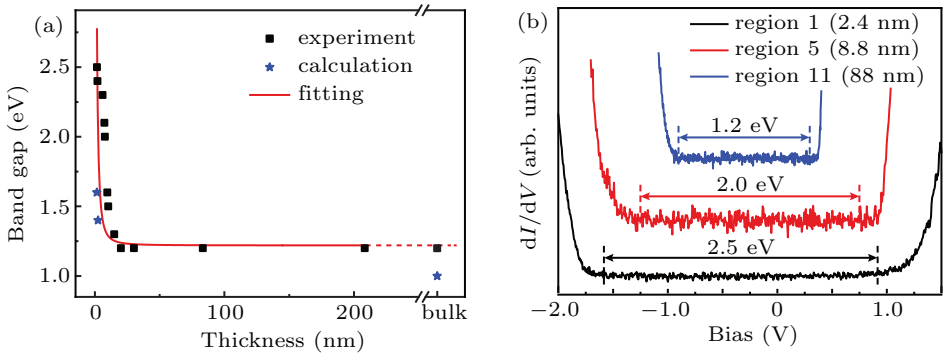


Fig. 2. (a) Thickness-dependent band-gap evolution in γ-InSe. Black squares (blue stars) represent the experimental (theoretical) results. The red curve is the fitting line of experimental results via the equation described in the main text. (b) Typical dI/dV spectra acquired in region 1 (black, 2.4 nm), 5 (red, 8.8 nm), and 11 (blue, 88 nm). The data have been offset for clarity.

After the exfoliation, a hexagonal moiré pattern induced by the rotated stack of surface and subsurface layers can also be observed in bulk γ-InSe [Fig. 3(a)]. The moiré periodicity of about 3.1 nm is derived from the height profile taken along the blue dashed line shown in Fig. 3(a). For two rotated lattices with the same lattice constant, the relationship between the moiré wavelength λ and the twist angle θ is given by the equation[44]

$$\lambda = \frac{a}{2\sin(\theta/2)}, \tag{4}$$

where a is the lattice constant. In our experiment, when the wavelength of the moiré pattern is 3.1 nm and the lattice constant is 0.4 nm for γ-InSe, the calculated twist angle between the surface and subsurface is about 7.3°. To illustrate the atomic structure of surface and subsurface layers of γ-InSe, we constructed a schematic lattice with a rotational angle $\sim 7.3°$ [Fig. 3(b)], which displays a moiré wavelength of 3.1 nm, and is in agreement with the experimental image [Fig. 3(a)].

Further comparative studies of the normally-stacked and moiré-pattern regions were performed by STS. The $\mathrm{d}I/\mathrm{d}V$ spectra measured with the same tip condition exhibit differences when the position changes between these two surfaces. Specifically, in the normally-stacked region, an electronic band gap of $E_g = 1.2$ eV is observed [red line in Fig. 3(c)], which is in line with previous experimental and theoretical results.[25,41,45] On the other hand, the band gap measured in the moiré-pattern region is slightly larger (~ 1.3 eV) [blue line in Fig. 3(c)]. A small variation (< 0.1 eV) of the band gap can also be seen in the calculated density of states (DOS) of 2QL γ-InSe with (blue curve) and without the twist angle (black curve) [Fig. 3(d)]. This indicates that the band gap is barely influenced by the induced moiré potential. The fact that the energy gap in the moiré-pattern region is close to that in bulk γ-InSe suggests that the surface layer is not decoupled, which evidences a considerable interlayer coupling between the surface and subsurface layers in γ-InSe.

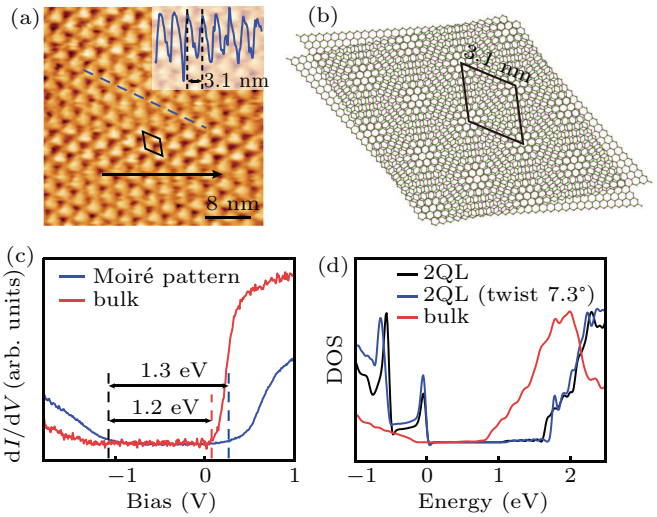


Fig. 3. (a) STM image (−2 V, 5 pA) acquired along the γ-InSe moiré pattern region. The black rhombus labels the moiré pattern primitive cell. The inset shows the height profile along the dashed blue line. (b) Schematic representation of a moiré pattern arising from a rotation angle $\theta = 7.3°$, (c) $\mathrm{d}I/\mathrm{d}V$ spectra (average of 10 repetitions) obtained on moiré pattern (blue curve) region and normal region (red curve) of γ-InSe. (d) Density of states calculated for 2QL γ-InSe (black curve), 2QL γ-InSe with 7.3° twist angle (blue curve), and bulk γ-InSe (red curve) using DFT. The Fermi level corresponds to the valence band edge.

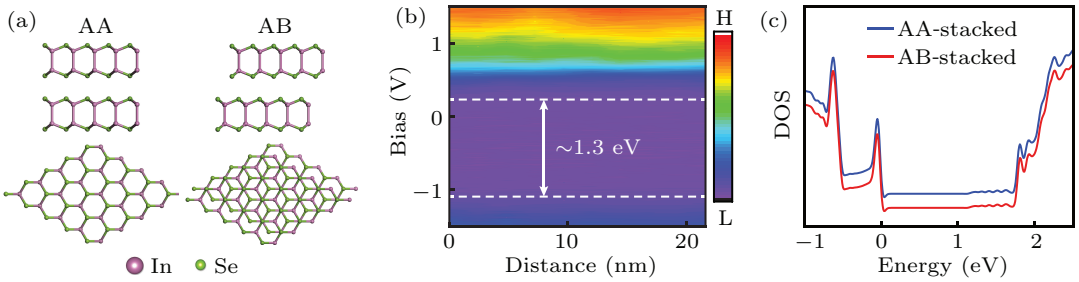


Fig. 4. (a) Atomic structure of AA and AB stackings. (b) A series of $\mathrm{d}I/\mathrm{d}V$ spectra measured along the direction showed by the black arrow (22 nm) in Fig. 3(a). Two dashed lines indicate the range of band gap. (c) Density of states calculated for AB-stacked (red curve) and AA-stacked (blue curve) 2QL γ-InSe with 7.3° twist angle. The Fermi level corresponds to the valence band edge. The data have been offset for clarity.

In the moiré-pattern region, two typical kinds of stacking, AA and AB, can be clearly identified with high and low apparent heights in STM images, respectively. These two stacking types are illustrated by ball-and-stick models with the side view (upper panel) and top view (lower panel) in Fig. 4(a). A strong interlayer coupling is additionally supported by the robust feature in a series of STS spectra measured along a 22-nm-long line crossing the moiré pattern region containing various types of stackings [Fig. 4(b)]. There are no obvious changes among all curves showing nearly constant band gaps similar to Fig. 3(c), and no new states can be observed. The calculated DOS of AA and AB stacked positions shown in Fig. 4(c) also demonstrates that there is negligible difference in the electronic structure between them. The stability of the electronic states across the moiré-pattern region is not typical for traditional TMD materials because the moiré-pattern potential field often induces an extra modulation of the electronic states.[46] Hence, strong interlayer coupling in γ-InSe is supposed to induce a smearing of the moiré potential modulation.

We further analyze the interlayer coupling in γ-InSe by a qualitative valence-bond theory. In γ-InSe, both Se and In atoms are coupled via the sp^3 hybridization. In this situation, each Se atom connects three other In atoms with three bonds located nearly in the same lattice plane (defined as x–y plane), which are known as sp-hybrid orbitals. Besides, Se atom provides paired electrons to form a p_z-like orbital (lone-pair) oriented perpendicular to the x–y plane (z direction). In turn, each In atom has four bonds, three of which are connected to Se atoms, and the remaining one couples two neighboring In atoms. Since the p_z-like orbital of Se is perpendicular to the lattice plane, the p_z-like electron cloud expands along the

z direction and extends out of the lattice plane. It is expected that the p_z-like orbitals overlap and strongly couple to each other.[41]

To support our analysis, we construct a set of the corresponding valence orbitals from our DFT calculations for 2QL γ-InSe. To this end, we utilize the maximally localized Wannier function procedure,[47] which allows one to transform the set of delocalized valence Bloch states into a set of localized bonding orbitals. The obtained orbitals are fully consistent with the qualitative analysis presented above. The most relevant p_z-like orbitals (lone-pairs) localized on Se atoms are schematically depicted in Fig. 5. In order to quantify the hybridization between the neighboring orbitals from different γ-InSe layers, we calculate the hopping integral $t_{12} = \langle \varphi_1(\boldsymbol{r}) | H | \varphi_2(\boldsymbol{r}) \rangle$, where $\varphi_1(\boldsymbol{r})$ and $\varphi_2(\boldsymbol{r})$ are Wannier orbitals associated with the lone-pairs shown in Fig. 5, and H is the electronic DFT Hamiltonian which describes the manifold of valence states in 2QL γ-InSe. The resulting hopping integral is $t_{12} \simeq -0.3$ eV, which is comparable in magnitude with that in graphite[48] and black phosphorus.[49] In contrast, t_{12} is negative indicating that the interlayer interaction in γ-InSe is energetically favorable from the electronic structure of view. This suggests that the interlayer coupling in γ-InSe is not of pure van der Waals origin, but demonstrates some degree of strong covalent bonding.

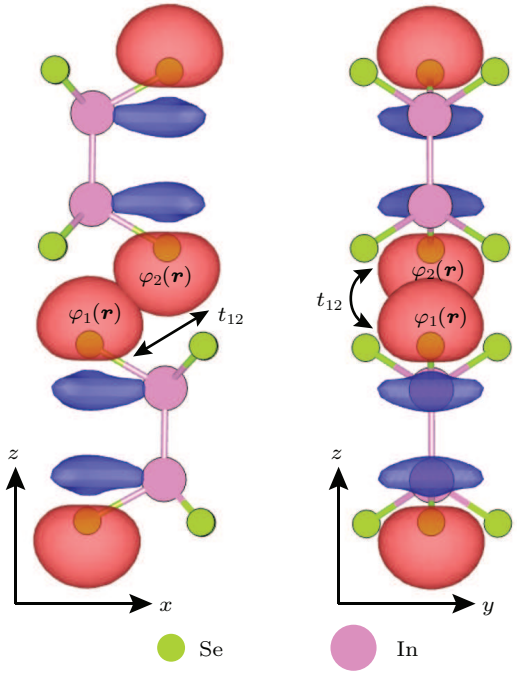


Fig. 5. A schematic representation of the valence orbitals localized on Se atoms in 2QL γ-InSe participating in hybridization between the layers. The green (purple) circle in the scheme represents Se (In).

5. Conclusion

In summary, we have studied the electronic properties of γ-InSe samples of various thickness using local differential conductivity measurements and DFT calculations. We have found a number of signatures of strong interlayer coupling in this layered material, which is revealed by the following observations. (1) Thickness-dependent band gap exhibits a sharp drop from ~ 2.5 to ~ 1.4 eV when the γ-InSe sample thickness increases up to 20 nm, which can barely be explained by quantum confinement effects. (2) The band gap is practically insensitive to the moiré potential, and is only slightly larger than that of normally-stacked bulk crystal. (3) Electronic states measured across the moiré-pattern regions do not show any significant difference among different stacking types. Our experimental results are in agreement with the valence-bond analysis supported by DFT calculations, which demonstrate a certain degree of hybridization between the layers, not typical to conventional van der Waals layered materials. These findings make a step forward in understanding the interlayer coupling in γ-InSe at the atomic level, and might be used in designing and fabricating devices based on this material.

Acknowledgment

We thank Dr. A. N. Rudenko for the help with theoretical calculations and Jing Wang, Yumu Yang, Ling-Hui Tong for experimental assistance.

References

[1] Huang B, Clark G, Navarro-Moratalla E, Klein D R, Cheng R, Seyler K L, Zhong D, Schmidgall E, McGuire M A, Cobden D H, Yao W, Xiao D, Jarillo-Herrero P and Xu X 2017 *Nature* **546** 270
[2] Wu Z B, Zhang Y Y, Li G, Du S X and Gao H J 2018 *Chin. Phys. B* **27** 077302
[3] Meng X Q, Chen S L, Fang Y Z and Kou J L 2019 *Chin. Phys. B* **28** 078101
[4] Heinrich B, Burrowes C, Montoya E, Kardasz B, Girt E, Song Y Y, Sun Y and Wu M 2011 *Phys. Rev. Lett.* **107** 066604
[5] Brihuega I, Mallet P, González-Herrero H, Trambly de Laissardière G, Ugeda M M, Magaud L, Gómez-Rodríguez J M, Ynduráin F and Veuillen J Y 2012 *Phys. Rev. Lett.* **109** 196802
[6] Qin Z H 2017 *Acta Phys. Sin.* **21** 216802 (in Chinese)
[7] Weller T E, Ellerby M, Saxena S S, Smith R P and Skipper N T 2005 *Nat. Phys.* **1** 39
[8] Guo Q M and Qin Z H 2021 *Acta Phys. Sin.* **70** 028101 (in Chinese)
[9] Bandurin D A, Tyurnina A V, Yu G L, Mishchenko A, Zolyomi V, Morozov S V, Kumar R K, Gorbachev R V, Kudrynskyi Z R, Pezzini S, Kovalyuk Z D, Zeitler U, Novoselov K S, Patane A, Eaves L, Grigorieva I V, Fal'ko V I, Geim A K and Cao Y 2017 *Nat. Nanotechnol.* **12** 223
[10] Tamalampudi S R, Lu Y Y, U R K, Sankar R, Liao C D, B K M, Cheng C H, Chou F C and Chen Y T 2014 *Nano Lett.* **14** 2800
[11] Kudrynskyi Z R, Bhuiyan M A, Makarovsky O, Greener J D G, Vdovin E E, Kovalyuk Z D, Cao Y, Mishchenko A, Novoselov K S, Beton P H, Eaves L and Patanè A 2017 *Phys. Rev. Lett.* **119** 157701
[12] Guo Y, Zhou S, Bai Y and Zhao J 2017 *Appl. Phys. Lett.* **110** 163102
[13] Liu L, Wu L, Wang A, Liu H, Ma R, Wu K, Chen J, Zhou Z, Tian Y, Yang H, Shen C, Bao L, Qin Z, Pantelides S T and Gao H J 2020 *Nano Lett.* **20** 6666
[14] Lugovskoi A V, Katsnelson M I and Rudenko A N 2019 *Phys. Rev. Lett.* **123** 176401
[15] Hung N T, Nugraha A R T and Saito R 2017 *Appl. Phys. Lett.* **111** 092107
[16] Mudd G W, Patanè A, Kudrynskyi Z R, Fay M W, Makarovsky O, Eaves L, Kovalyuk Z D, Zólyomi V and Falko V 2014 *Appl. Phys. Lett.* **105** 221909
[17] Kibirev I A, Matetskiy A V, Zotov A V and Saranin A A 2018 *Appl. Phys. Lett.* **112** 191602

[18] Sun Y, Luo S, Zhao X G, Biswas K, Li S L and Zhang L 2018 *Nanoscale* **10** 7991

[19] Song C, Fan F, Xuan N, Huang S, Zhang G, Wang C, Sun Z, Wu H and Yan H 2018 *ACS Appl. Mater. Interfaces* **10** 3994

[20] Li W, Poncé S and Giustino F 2019 *Nano Lett.* **19** 1774

[21] Mudd G W, Svatek S A, Ren T, Patanè A, Makarovsky O, Eaves L, Beton P H, Kovalyuk Z D, Lashkarev G V, Kudrynskyi Z R and Dmitriev A I 2013 *Adv. Mater.* **25** 5714

[22] Mudd G W, Molas M R, Chen X, Zólyomi V, Nogajewski K, Kudrynskyi Z R, Kovalyuk Z D, Yusa G, Makarovsky O, Eaves L, Potemski M, Fal'ko V I and Patanè A 2016 *Sci. Rep.* **6** 39619

[23] Zhang Z, Chen Z, Bouaziz M, Giorgetti C, Yi H, Avila J, Tian B, Shukla A, Perfetti L, Fan D, Li Y and Bendounan A 2019 *ACS Nano* **13** 13486

[24] Chen Z, Giorgetti C, Sjakste J, Cabouat R, Véniard V, Zhang Z, Taleb-Ibrahimi A, Papalazarou E, Marsi M, Shukla A, Peretti J and Perfetti L 2018 *Phys. Rev. B* **97** 241201

[25] Henck H, Pierucci D, Zribi J, Bisti F, Papalazarou E, Girard J C, Chaste J, Bertran F, Le Fèvre P, Sirotti F, Perfetti L, Giorgetti C, Shukla A, Rault J E and Ouerghi A 2019 *Phys. Rev. Mater.* **3** 034004

[26] Li S, Zhong C, Henning A, Sangwan V K, Zhou Q, Liu X, Rahn M S, Wells S A, Park H Y, Luxa J, Sofer Z, Facchetti A, Darancet P, Marks T J, Lauhon L J, Weiss E A and Hersam M C 2020 *ACS Nano* **14** 3509

[27] Zhang S, Wang C G, Li M Y, Huang D, Li L J, Ji W and Wu S 2017 *Phys. Rev. Lett.* **119** 046101

[28] Yin L J, Yang L Z, Zhang L, Wu Q, Fu X, Tong L H, Yang G, Tian Y, Zhang L and Qin Z 2020 *Phys. Rev. B* **102** 241403

[29] Huang Y, Pan Y H, Yang R, *et al.* 2020 *Nat. Commun.* **11** 2453

[30] Horcas I, Fernández R, Gómez-Rodríguez J M, Colchero J, Gómez-Herrero J and Baro A M 2007 *Rev. Sci. Instrum.* **78** 013705

[31] Blöchl P E 1994 *Phys. Rev. B* **50** 17953

[32] Kresse G and Furthmüller J 1996 *Phys. Rev. B* **54** 11169

[33] Kresse G and Joubert D 1999 *Phys. Rev. B* **59** 1758

[34] Wijk M M v, Schuring A, Katsnelson M I and Fasolino A 2015 *2D Mater.* **2** 034010

[35] Pizzi G, Vitale V, Arita R, *et al.* 2020 *J. Phys.: Condens. Matter* **32** 165902

[36] Dai M, Chen H, Wang F, Hu Y, Wei S, Zhang J, Wang Z, Zhai T and Hu P 2019 *ACS Nano* **13** 7291

[37] Errandonea D, Segura A, Manjón F J, Chevy A, Machado E, Tobias G, Ordejón P and Canadell E 2005 *Phys. Rev. B* **71** 125206

[38] Zeng J, He X, Liang S J, Liu E, Sun Y, Pan C, Wang Y, Cao T, Liu X, Wang C, Zhang L, Yan S, Su G, Wang Z, Watanabe K, Taniguchi T, Singh D J, Zhang L and Miao F 2018 *Nano Lett.* **18** 7538

[39] Zhao Y, Qiao J, Yu P, Hu Z, Lin Z, Lau S P, Liu Z, Ji W and Chai Y 2016 *Adv. Mater.* **28** 2399

[40] Shubina T V, Desrat W, Moret M, Tiberj A, Briot O, Davydov V Y, Platonov A V, Semina M A and Gil B 2019 *Nat. Commun.* **10** 3479

[41] Magorrian S J, Zólyomi V and Fal'ko V I 2016 *Phys. Rev. B* **94** 245431

[42] Weiser G 1992 *Phys. Rev. B* **45** 14076

[43] Li W and Giustino F 2020 *Phys. Rev. B* **101** 035201

[44] Miller D L, Kubista K D, Rutter G M, Ruan M, de Heer W A, First P N and Stroscio J A 2010 *Phys. Rev. B* **81** 125427

[45] Hamer M J, Zultak J, Tyurnina A V, Zolyomi V, Terry D, Barinov A, Garner A, Donoghue J, Rooney A P, Kandyba V, Giampietri A, Graham A, Teutsch N, Xia X, Koperski M, Haigh S J, Fal'ko V I, Gorbachev R V and Wilson N R 2019 *ACS Nano* **13** 2136

[46] Lu J, Bao D L, Qian K, Zhang S, Chen H, Lin X, Du S X and Gao H J 2017 *ACS Nano* **11** 1689

[47] Marzari N, Mostofi A A, Yates J R, Souza I and Vanderbilt D 2012 *Rev. Mod. Phys.* **84** 1419

[48] Grüneis A, Attaccalite C, Wirtz L, Shiozawa H, Saito R, Pichler T and Rubio A 2008 *Phys. Rev. B* **78** 205425

[49] Rudenko A N, Yuan S and Katsnelson M I 2015 *Phys. Rev. B* **92** 085419